

1 A General Analytical Model for Head Response to Oscillatory Pumping in

2 Unconfined Aquifers: Effects of Delayed Gravity Drainage and Initial

3 Condition

4 Ching-Sheng Huang^a, Ya-Hsin Tsai^b, Hund-Der Yeh^{b*} and Tao Yang^{a*}

⁵ ^a State Key Laboratory of Hydrology-Water Resources and Hydraulic Engineering, Center for
⁶ Global Change and Water Cycle, Hohai University, Nanjing 210098, China

⁷ ^b Institute of Environmental Engineering, National Chiao Tung University, Hsinchu 300,
⁸ Taiwan

9 * Corresponding authors:

10 Hund-Der Yeh; E-mail: hdye@ntu.edu.tw; Tel.: +886-3-5731910; fax: +886-3-
11 5725958

12 Tao Yang; E-mail: tao.yang@hhu.edu.cn; Tel.: +86-13770918075

13 Submission to *Hydrology and Earth System Sciences* on 11 September 2018

14 Re-submission to *Hydrology and Earth System Sciences* on 24 December 2018

15 Re-re-submission to *Hydrology and Earth System Sciences* on 27 February 2019

16 Key points

17 1. An analytical model of the hydraulic head due to oscillatory pumping in unconfined
18 aquifers is presented.

19 2. Head fluctuations affected by instantaneous and delayed gravity drainages are discussed.

20 3. The effect of initial condition on the phase of head fluctuation is analyzed.

21 4. The present solution agrees well to head fluctuation data taken from a field oscillatory
22 pumping.

Abstract

Oscillatory pumping tests (OPTs) provide an alternative to constant-head and constant-rate pumping tests for determining aquifer hydraulic parameters when OPT data are analyzed based on an associated analytical model coupled with an optimization approach. There is a large number of analytical models presented for the analysis of OPT. The combined effects of delayed gravity drainage (DGD) and initial condition regarding the hydraulic head are commonly neglected in the existing models. This study aims to develop a new model for describing the hydraulic head fluctuation induced by OPT in an unconfined aquifer. The model contains a groundwater flow equation with the initial condition of static water table, Neumann boundary condition specified at the rim of a partially screened well, and a free surface equation describing water table motion with the DGD effect. The solution is derived using the Laplace, finite-integral, and Weber transforms. Sensitivity analysis is carried out for exploring head response to the change in each of hydraulic parameters. Results suggest the DGD reduces to instantaneous gravity drainage in predicting transient head fluctuation when dimensionless parameter $a_1 = \epsilon S_y b / K_z$ exceeds 500 with empirical constant ϵ , specific yield S_y , aquifer thickness b , and vertical hydraulic conductivity K_z . The water table can be regarded as a no-flow boundary when $a_1 < 10^{-2}$ and $P < 10^4$ s with P being the period of oscillatory pumping rate. A pseudo-steady state model without initial condition causes a time shift from the actual transient model in predicting simple harmonic motion of head fluctuation during a late pumping period. In addition, the present solution agrees well to head fluctuation data observed at the Savannah River site.

KEYWORDS: oscillatory pumping test, analytical solution, free surface equation, delayed gravity drainage, initial condition

Notation and Abbreviation

a	$bD_r/(C_y r_w^2)$
a_1, a_2	$b/(\kappa C_y), r_w^2/(\kappa D_r)$
b	Aquifer thickness
C_y	K_z/S_y
D_r	K_r/S_s
DGD	Delayed gravity drainage
h	Hydraulic head
\bar{h}	Dimensionless Hydraulic head, i.e., $\bar{h} = 2\pi l K_r h / Q$
IGD	Instantaneous gravity drainage
K_r, K_z	Aquifer horizontal and vertical hydraulic conductivities, respectively
LHS	Left-hand side
l	Screen length, i.e., $z_u - z_l$
OPT	oscillatory pumping test
P	Period of oscillatory pumping rate
PSS	Pseudo-steady state
\bar{P}	Dimensionless period, i.e., $\bar{P} = D_r P / r_w^2$
p	Laplace parameter
Q	Amplitude of oscillatory pumping rate
RHS	Right-hand side
r	Radial distance from the center of pumping well
\bar{r}	Dimensionless radial distance, i.e., $\bar{r} = r/r_w$
r_w	Radius of pumping well
SHM	Simple harmonic motion
S_s, S_y	Specific storage and specific yield, respectively
t	Time since pumping
\bar{t}	Dimensionless pumping time, i.e., $\bar{t} = D_r t / r_w^2$
z	Elevation from aquifer bottom
z_l, z_u	Lower and upper elevations of well screen, respectively
\bar{z}	Dimensionless elevation, i.e., $\bar{z} = z/b$
\bar{z}_l, \bar{z}_u	$z_l/b, z_u/b$
α	K_z/K_r
β_n	Roots of Eq. (15)
κ	$1/\epsilon$
γ	Dimensionless frequency of oscillatory pumping rate, i.e., $\omega r_w^2 / D_r$
ϵ	Empirical constant associated with delayed gravity drainage
μ	$\alpha r_w^2 / b^2$
ω	Frequency of oscillatory pumping rate, i.e., $\omega = 2\pi/P$

48 **1. Introduction**

49 Numerous attempts have been made by researchers to the study of oscillatory pumping test
50 (OPT) that is an alternative to constant-rate and constant-head pumping tests for determining
51 aquifer hydraulic parameters (e.g., Vine et al., 2016; Christensen et al., 2017; Watlet et al.,
52 2018). The concept of OPT was first proposed by Kuo (1972) in the petroleum literature. The
53 process of OPT contains extraction stages and injection stages. The pumping rate, in other
54 words, varies periodically as a sinusoidal function of time. Compared with traditional constant-
55 rate pumping, OPT in contaminated aquifers has the following advantages: (1) low cost because
56 of no disposing contaminated water from the well, (2) reduced risk of treating contaminated
57 fluid, (3) smaller contaminant movement, and (4) stable signal easily distinguished from
58 background disturbance such as tide effect and varying river stage (e.g., Spane and Mackley,
59 2011). However, the disadvantages of OPT include the need of an advanced apparatus
60 producing periodic rate. Oscillatory hydraulic tomography adopts several oscillatory pumping
61 wells with different frequencies (e.g., Yeh and Liu, 2000; Cardiff et al., 2013; Zhou et al., 2016;
62 Muthuwatta et al., 2017). Aquifer heterogeneity can be mapped by analyzing multiple data
63 collected from observation wells. Cardiff and Barrash (2011) reviewed articles associated with
64 hydraulic tomography and classified them according to nine categories in a table.

65 Various groups of researchers have worked with analytical and numerical models for OPT;
66 each group has its own model and investigation. For example, Black and Kipp (1981) assumed
67 the response of confined flow to OPT as simple harmonic motion (SHM) in the absence of
68 initial condition. Cardiff and Barrash (2014) built an optimization formulation strategy using
69 the Black and Kipp analytical solution. Dagan and Rabinovich (2014) also assumed hydraulic
70 head fluctuation as SHM for OPT at a partially screened well in unconfined aquifers. Cardiff
71 et al. (2013) characterized aquifer heterogeneity using the finite element-based COMSOL
72 software that adopts SHM hydraulic head variation for OPT. On the other hand, Rasmussen et
73 al. (2003) found hydraulic head response tends to SHM at a late period of pumping time when

74 considering initial condition prior to OPT. Bakhos et al. (2014) used the Rasmussen et al. (2003)
75 analytical solution to quantify the time after which hydraulic head fluctuation can be regarded
76 as SHM since OPT began. As mentioned above, most of the models for OPT assume hydraulic
77 head fluctuation as SHM without initial condition, and all of them treat the pumping well as a
78 line source with infinitesimal radius.

79 Field applications of OPT for determining aquifer parameters have been conducted in
80 recent years. Rasmussen et al. (2003) estimated aquifer hydraulic parameters based on 1- or 2-
81 hour period of OPT at the Savannah River site. Maineult et al. (2008) observed spontaneous
82 potential temporal variation in aquifer diffusivity at a study site in Bochum, Germany. Fokker
83 et al. (2012; 2013) presented spatial distributions of aquifer transmission and storage
84 coefficient derived from curve fitting based on a numerical model and field data from
85 experiments at the southern city-limits of Bochum, Germany. Rabinovich et al. (2015)
86 estimated aquifer parameters of equivalent hydraulic conductivity, specific storage and specific
87 yield at the Boise Hydrogeophysical Research Site by curve fitting based on observation data
88 and the Dagan and Rabinovich (2014) analytical solution. They conclude the equivalent
89 hydraulic parameters can represent the actual aquifer heterogeneity of the study site.

90 Although a large number of studies have been made in developing analytical models for
91 OPT, little is known about the combined effects of delayed gravity drainage (DGD), finite-
92 radius pumping well, and initial condition prior to OPT. Analytical solution to such a question
93 will not only have important physical implications but also shed light on OPT model
94 development. This study builds an improved model describing hydraulic head fluctuation
95 induced by OPT in an unconfined aquifer. The model is composed of a typical flow equation
96 with the initial condition of static water table, an inner boundary condition specified at the rim
97 of the partially screened well for incorporating finite-radius effect, and a free surface equation
98 describing the motion of water table with the DGD effect. The analytical solution of the model
99 is derived by the methods of Laplace transform, finite-integral transform, and Weber transform.

100 Based on the present solution, sensitivity analysis is performed to explore the hydraulic head
 101 in response to the change in each of hydraulic parameters. The effects of DGD and
 102 instantaneous gravity drainage (IGD) on the head fluctuations are compared. The quantitative
 103 criterion for treating the well radius as infinitesimal is discussed. The effect of the initial
 104 condition on the phase of head fluctuation is investigated. In addition, curve fitting of the
 105 present solution to head fluctuation data recorded at the Savannah River site is presented.

106 **2. Methodology**

107 **2.1. Mathematical model**

108 Consider an OPT in an unconfined aquifer illustrated in Fig. 1. The aquifer is of unbound lateral
 109 extent with a finite thickness b . The radial distance from the centerline of the well is r ; an
 110 elevation from the impermeable bottom of the aquifer is z . The well with outer radius r_w is
 111 screened from elevation z_u to z_l .

112 The flow equation describing spatiotemporal head distribution in aquifers can be written
 113 as:

$$114 D_r \left(\frac{\partial^2 h}{\partial r^2} + \frac{1}{r} \frac{\partial h}{\partial r} + \alpha \frac{\partial^2 h}{\partial z^2} \right) = \frac{\partial h}{\partial t} \quad \text{for } r_w \leq r < \infty, 0 \leq z \leq b \text{ and } t \geq 0 \quad (1)$$

115 where $D_r = K_r/S_s$; $\alpha = K_z/K_r$; $h(r, z, t)$ is hydraulic head at location (r, z) and time t ; K_r
 116 and K_z are respectively the radial and vertical hydraulic conductivities; S_s is the specific
 117 storage. Consider water table as a reference datum where the elevation head is set to zero; the
 118 initial condition is expressed as:

$$119 h = 0 \text{ at } t = 0 \quad (1)$$

120 The rim of the wellbore is regarded as an inner boundary under the Neumann condition
 121 expressed as:

$$122 2\pi r_w K_r l \frac{\partial h}{\partial r} = \begin{cases} Q \sin(\omega t) & \text{for } z_l \leq z \leq z_u \\ 0 & \text{outside screen interval} \end{cases} \quad \text{at } r = r_w \quad (2)$$

123 where $l = z_u - z_l$ is screen length; Q and $\omega = 2\pi/P$ are respectively the amplitude and
 124 frequency of oscillatory pumping rate (i.e., $Q \sin(\omega t)$) with a period P . Water table motion can

125 be defined by Eq. (4a) for IGD (Neuman, 1972) and Eq. (4b) for DGD (Moench, 1995).

126 $\frac{\partial h}{\partial z} = -\frac{1}{C_y} \frac{\partial h}{\partial t} \text{ at } z = b \text{ for IGD}$ (3a)

127 $\frac{\partial h}{\partial z} = \frac{1}{\kappa C_y} \int_0^t \frac{\partial h}{\partial \tau} \exp(-(t - \tau)/\kappa) d\tau \text{ at } z = b \text{ for DGD}$ (4b)

128 where $C_y = K_z/S_y$, $\kappa = 1/\epsilon$ with ϵ being an empirical constant, and S_y is the specific
129 yield. Note that Eq. (4b) reduces to Eq. (4a) when $\kappa \rightarrow \infty$ or $\epsilon = 0$. The impervious aquifer
130 bottom is under the no-flow condition:

131 $\frac{\partial h}{\partial z} = 0 \text{ at } z = 0$ (4)

132 The hydraulic head far away from the pumping well remains constant, written as

133 $\lim_{r \rightarrow \infty} h(r, z, t) = 0$ (5)

134 Define dimensionless variables and parameters as follows:

135 $\bar{h} = \frac{2\pi l K_r}{Q} h, \bar{r} = \frac{r}{r_w}, \bar{z} = \frac{z}{b}, \bar{z}_l = \frac{z_l}{b}, \bar{z}_u = \frac{z_u}{b}, \bar{t} = \frac{D_r}{r_w^2} t, \bar{\tau} = \frac{D_r}{r_w^2} \tau, \bar{P} = \frac{D_r}{r_w^2} P$

136 $\gamma = \frac{\omega r_w^2}{D_r}, \mu = \frac{\alpha r_w^2}{b^2}, a = \frac{b D_r}{C_y r_w^2}, a_1 = \frac{b}{\kappa C_y}, a_2 = \frac{r_w^2}{\kappa D_r}$ (6)

137 where the overbar stands for a dimensionless symbol. Note that the magnitude of a_1 is related
138 to the DGD effect (Moench, 1995) and γ is a dimensionless frequency parameter. With Eq. (7),
139 the dimensionless forms of Eqs. (1) - (6) become, respectively,

140 $\frac{\partial^2 \bar{h}}{\partial \bar{r}^2} + \frac{1}{\bar{r}} \frac{\partial \bar{h}}{\partial \bar{r}} + \mu \frac{\partial^2 \bar{h}}{\partial \bar{z}^2} = \frac{\partial \bar{h}}{\partial \bar{t}} \text{ for } 1 \leq \bar{r} < \infty, 0 \leq \bar{z} < 1 \text{ and } \bar{t} \geq 0$ (7)

141 $\bar{h} = 0 \text{ at } \bar{t} = 0$ (8)

142 $\frac{\partial \bar{h}}{\partial \bar{r}} = \begin{cases} \sin(\gamma \bar{t}) & \text{for } \bar{z}_l \leq \bar{z} \leq \bar{z}_u \\ 0 & \text{outside screen interval} \end{cases} \text{ at } \bar{r} = 1$ (9)

143 $\frac{\partial \bar{h}}{\partial \bar{z}} = -a \frac{\partial \bar{h}}{\partial \bar{t}} \text{ at } \bar{z} = 1 \text{ for IGD}$ (10a)

144 $\frac{\partial \bar{h}}{\partial \bar{z}} = -a_1 \int_0^{\bar{t}} \frac{\partial \bar{h}}{\partial \bar{\tau}} \exp(-a_2(\bar{t} - \bar{\tau})) d\bar{\tau} \text{ at } \bar{z} = 1 \text{ for DGD}$ (11b)

145 $\frac{\partial \bar{h}}{\partial \bar{z}} = 0 \text{ at } \bar{z} = 0$ (12)

146 $\lim_{\bar{r} \rightarrow \infty} \bar{h}(\bar{r}, \bar{z}, \bar{t}) = 0$ (13)

147 Eqs. (8) – (13) represent the transient DGD model when excluding (11a) and transient IGD
 148 model when excluding (11b).

149 **2.2. Transient solution for unconfined aquifer**

150 The Laplace transform and finite-integral transform are applied to solve Eqs. (8) - (13)
 151 (Latinopoulos, 1985; Liang et al., 2017; 2018). The transient solution can then be expressed as

152 $\bar{h}(\bar{r}, \bar{z}, \bar{t}) = \bar{h}_{\text{exp}}(\bar{r}, \bar{z}, \bar{t}) + \bar{h}_{\text{SHM}}(\bar{r}, \bar{z}, \bar{t})$ (14a)

153 with

154 $\bar{h}_{\text{exp}}(\bar{r}, \bar{z}, \bar{t}) = \frac{-2\gamma}{\pi} \sum_{n=1}^{\infty} \int_0^{\infty} \cos(\beta_n \bar{z}) \exp(p_0 \bar{t}) \text{Im}(\varepsilon_1 \varepsilon_2) d\zeta$ (14b)

155 $\bar{h}_{\text{SHM}}(\bar{r}, \bar{z}, \bar{t}) = \bar{A}_t(\bar{r}, \bar{z}) \cos(\gamma \bar{t} - \phi_t(\bar{r}, \bar{z}))$ (14c)

156 $\bar{A}_t(\bar{r}, \bar{z}) = \sqrt{a_t(\bar{r}, \bar{z})^2 + b_t(\bar{r}, \bar{z})^2}$ (14d)

157 $a_t(\bar{r}, \bar{z}) = \frac{2}{\pi} \sum_{n=1}^{\infty} \int_0^{\infty} p_0 \cos(\beta_n \bar{z}) \text{Im}(\varepsilon_1 \varepsilon_2) d\zeta$ (14e)

158 $b_t(\bar{r}, \bar{z}) = \frac{2\gamma}{\pi} \sum_{n=1}^{\infty} \int_0^{\infty} \cos(\beta_n \bar{z}) \text{Im}(\varepsilon_1 \varepsilon_2) d\zeta$ (14f)

159 $\phi_t(\bar{r}, \bar{z}) = \cos^{-1}(b_t(\bar{r}, \bar{z})/\bar{A}_t(\bar{r}, \bar{z}))$ (14g)

160 $\varepsilon_1 = K_0(\lambda_0 \bar{r})(\sin(\bar{z}_u \beta_n) - \sin(\bar{z}_l \beta_n)) / (\beta_n \lambda_0 K_1(\lambda_0)(p_0^2 + \gamma^2))$ (14h)

161 $\varepsilon_2 = (\beta_n^2 + c_0^2) / (\beta_n^2 + c_0^2 + c_0)$ (14i)

162 $p_0 = -\zeta - \mu \beta_n^2$ (14j)

163 $\lambda_0 = \sqrt{\zeta} i$ (14k)

164 where $c_0 = a p_0$ for IGD and $a_1 p_0 / (p_0 + a_2)$ for DGD, i is the imaginary unit, $\text{Im}(-)$ is the
 165 imaginary part of a complex number, $K_0(-)$ and $K_1(-)$ are the modified Bessel functions
 166 of the second kind of order zero and one, respectively, and β_n is the positive roots of the
 167 equation:

168 $\tan \beta_n = c_0 / \beta_n$ (15)

169 The method to find the roots of β_n is discussed in Section 2.3. The detailed derivation of
 170 Eqs. (14a) – (14k) is presented in the supporting material. The first term on the right-hand side
 171 (RHS) of Eq. (14a) exhibits exponential decay due to the initial condition since pumping began;

172 the second term defines SHM with amplitude $\bar{A}_t(\bar{r}, \bar{z})$ and phase shift $\phi_t(\bar{r}, \bar{z})$ at a given
 173 point (\bar{r}, \bar{z}) . The numerical results of the integrals in Eqs. (14b), (14e) and (14f) are obtained
 174 by the Mathematica NIntegrate function.

175 **2.3. Calculation of β_n**

176 The eigenvalues β_1, \dots, β_n , the roots of Eq. (15) can be determined by applying the
 177 Mathematica function FindRoot based on Newton's method with reasonable initial guesses.
 178 The roots are located at the intersection of the curves plotted by the RHS and left-hand side
 179 (LHS) functions of β_n in Eq. (15). The roots are very close to the vertical asymptotes of the
 180 periodical tangent function $\tan \beta_n$. When $c_0 = ap_0$, the initial guess for each β_n can be
 181 considered as $\beta_{0,n} + \delta$ where $\beta_{0,n} = (2n - 1)\pi/2$, $n \in (1, 2, \dots, \infty)$ and δ is a small
 182 positive value set to 10^{-10} . When $c_0 = a_1 p_0 / (p_0 + a_2)$, the initial guess is set to $\beta_{0,n} - \delta$ for
 183 $a_2 - \zeta \leq 0$. There is an additional vertical asymptote at $\beta_n = \sqrt{(a_2 - \zeta)/\mu}$ derived from the
 184 RHS function of Eq. (15) (i.e., $p_0 + a_2 = 0$) if $a_2 - \zeta > 0$. The initial guess is therefore set
 185 to $\beta_{0,n} + \delta$ for $\beta_{0,n}$ on the LHS of the asymptote and $\beta_{0,n} - \delta$ for $\beta_{0,n}$ on the RHS.

186 **2.4. Transient solution for confined aquifer**

187 When $S_y = 0$ (i.e., $a = 0$ or $a_1 = 0$), Eq. (11a) or (11b) reduces to $\partial \bar{h} / \partial \bar{z} = 0$ for no-flow
 188 condition at the top of the aquifer, indicating the unconfined aquifer becomes a confined one.
 189 Under this condition, Eq. (15) becomes $\tan \beta_n = 0$ with roots $\beta_n = 0, \pi, 2\pi, \dots, n\pi, \dots,$
 190 ∞ ; Eq. (14i) reduces to $\varepsilon_2 = 1$; factor 2 in Eqs. (14b), (14e) and (14f) is replaced by unity for
 191 $\beta_n = 0$ and remains for the others. The analytical solution of the transient head for the
 192 confined aquifer can be expressed as Eqs. (14a) - (14k) with

$$193 \bar{h}_{\text{exp}}(\bar{r}, \bar{z}, \bar{t}) = \frac{-\gamma}{\pi} \int_0^\infty \text{Im}(\varepsilon_0) \exp(-\zeta \bar{t}) d\zeta - \frac{2\gamma}{\pi} \sum_{n=1}^{\infty} \int_0^\infty \cos(n\pi \bar{z}) \text{Im}(\varepsilon_1) \exp(p_0 \bar{t}) d\zeta \quad (16a)$$

$$195 a_t(\bar{r}, \bar{z}) = -\frac{1}{\pi} \int_0^\infty \zeta \text{Im}(\varepsilon_0) d\zeta + \frac{2}{\pi} \sum_{n=1}^{\infty} \int_0^\infty p_0 \cos(n\pi \bar{z}) \text{Im}(\varepsilon_1) d\zeta \quad (16b)$$

196 $b_t(\bar{r}, \bar{z}) = \frac{\gamma}{\pi} \int_0^\infty \text{Im}(\varepsilon_0) d\zeta + \frac{2\gamma}{\pi} \sum_{n=1}^\infty \int_0^\infty \cos(n\pi\bar{z}) \text{Im}(\varepsilon_1) d\zeta$ (16c)

197 $\varepsilon_0 = (\bar{z}_u - \bar{z}_l) K_0(\lambda_0 \bar{r}) / (\lambda_0 K_1(\lambda_0)(\zeta^2 + \gamma^2))$ (16d)

198 Note that Eq. (14h) reduces to Eq. (16d) based on $\beta_n = 0$ and L' Hospital's rule. When
 199 $\bar{z}_u = 1$ and $\bar{z}_l = 0$ for the case of full screen, Eq. (14h) gives $\varepsilon_1 = 0$ for $\beta_n > 0$ and the
 200 second RHS terms of Eqs. (16a) – (16c) can therefore be eliminated. This causes the solution
 201 for confined aquifers is independent of dimensionless elevation \bar{z} , indicating only horizontal
 202 flow in the aquifer.

203 **2.5. Pseudo-steady state solution for unconfined aquifer**

204 A pseudo-steady state (PSS) solution \bar{h}_s accounts for SHM of head fluctuation at a late period
 205 of pumping time and satisfies the following form (Dagan and Rabinovich, 2014)

206 $\bar{h}_s(\bar{r}, \bar{z}, \bar{t}) = \text{Im}(\bar{H}(\bar{r}, \bar{z}) e^{i\gamma\bar{t}})$ (17)

207 where $\bar{H}(\bar{r}, \bar{z})$ is a space function of \bar{r} and \bar{z} . Define a PSS IGD model as Eqs. (8) - (13)
 208 excluding (9), (11b) and replacing $\sin(\gamma\bar{t})$ in (10) by $e^{i\gamma\bar{t}}$. Substituting Eq. (17) and
 209 $\partial\bar{h}_s/\partial\bar{t} = \text{Im}(i\gamma\bar{H}(\bar{r}, \bar{z}) e^{i\gamma\bar{t}})$ into the model results in

210 $\frac{\partial^2 \bar{H}}{\partial \bar{r}^2} + \frac{1}{\bar{r}} \frac{\partial \bar{H}}{\partial \bar{r}} + \mu \frac{\partial^2 \bar{H}}{\partial \bar{z}^2} = i\gamma \bar{H}$ (18)

211 $\frac{\partial \bar{H}}{\partial \bar{r}} = \begin{cases} 1 & \text{for } \bar{z}_l \leq \bar{z} \leq \bar{z}_u \\ 0 & \text{outside screen interval} \end{cases} \text{ at } \bar{r} = 1$ (19)

212 $\frac{\partial \bar{H}}{\partial \bar{z}} = -iay\bar{H} \text{ at } \bar{z} = 1 \text{ for IGD}$ (20)

213 $\frac{\partial \bar{H}}{\partial \bar{z}} = 0 \text{ at } \bar{z} = 0$ (21)

214 $\lim_{\bar{r} \rightarrow \infty} \bar{H} = 0$ (22)

215 The resultant model is independent of \bar{t} , indicating the analytical solution of $\bar{H}(\bar{r}, \bar{z})$ is
 216 tractable. Similarly, consider a PSS DGD model that equals the PSS IGD model but replaces
 217 (11a) by (11b). Substituting Eq. (17) into the result yields a model that depends on \bar{t} , indicating
 218 the solution \bar{h}_s to the PSS DGD model is not tractable.

219 The Weber transform, defined in Eq. (B.1) of the supporting material, may be considered

220 as a Hankel transform with a more general kernel function. It can be applied to diffusion-type
 221 problems with a radial-symmetric region from a finite distance to infinity. For groundwater
 222 flow problems, it can be used to develop the analytical solution for the flow equation with a
 223 Neumann boundary condition specified at the rim of a finite-radius well (e.g., Lin and Yeh,
 224 2017; Povstenko, 2015). Taking the transform and the formula of $e^{i\gamma\bar{t}} = \cos(\gamma\bar{t}) + i \sin(\gamma\bar{t})$
 225 to solve Eqs. (18) - (22) yields the solution of \bar{h}_s expressed as

$$226 \quad \bar{h}_s(\bar{r}, \bar{z}, \bar{t}) = \bar{A}_s(\bar{r}, \bar{z}) \cos(\gamma t - \phi_s(\bar{r}, \bar{z})) \quad (23a)$$

$$227 \quad \bar{A}_s(\bar{r}, \bar{z}) = \sqrt{a_s(\bar{r}, \bar{z})^2 + b_s(\bar{r}, \bar{z})^2} \quad (23b)$$

$$228 \quad a_s(\bar{r}, \bar{z}) = \operatorname{Re}(\bar{H}(\bar{r}, \bar{z})) \quad (23c)$$

$$229 \quad b_s(\bar{r}, \bar{z}) = \operatorname{Im}(\bar{H}(\bar{r}, \bar{z})) \quad (23d)$$

$$230 \quad \phi_s(\bar{r}, \bar{z}) = \cos^{-1}(b_s(\bar{r}, \bar{z})/A_s(\bar{r}, \bar{z})) \quad (23e)$$

$$231 \quad \bar{H}(\bar{r}, \bar{z}) = \begin{cases} \int_0^\infty \tilde{H}_u \xi \Omega d\xi & \text{for } \bar{z}_u < \bar{z} \leq 1 \\ \int_0^\infty \tilde{H}_m \xi \Omega d\xi & \text{for } \bar{z}_l \leq \bar{z} \leq \bar{z}_u \\ \int_0^\infty \tilde{H}_l \xi \Omega d\xi & \text{for } 0 \leq \bar{z} < \bar{z}_l \end{cases} \quad (23f)$$

$$232 \quad \Omega = (J_0(\xi\bar{r})Y_1(\xi) - Y_0(\xi\bar{r})J_1(\xi))/(J_1^2(\xi) + Y_1^2(\xi)) \quad (23g)$$

233 with the Bessel functions of the first kind of order zero $J_0(-)$ and one $J_1(-)$ as well as the
 234 second kind of order zero $Y_0(-)$ and one $Y_1(-)$,

$$235 \quad \begin{cases} \tilde{H}_u = \tilde{H}_p(c_1 \exp(\lambda_w \bar{z}) + c_2 \exp(-\lambda_w \bar{z})) & \text{for } \bar{z}_u < \bar{z} \leq 1 \\ \tilde{H}_m = \tilde{H}_p(c_3 \exp(\lambda_w \bar{z}) + c_4 \exp(-\lambda_w \bar{z}) - 1) & \text{for } \bar{z}_l \leq \bar{z} \leq \bar{z}_u \\ \tilde{H}_l = \tilde{H}_p c_5(\exp(\lambda_w \bar{z}) + \exp(-\lambda_w \bar{z})) & \text{for } 0 \leq \bar{z} < \bar{z}_l \end{cases} \quad (23h)$$

$$236 \quad c_1 = -e^{-\lambda_w}(\lambda_w - \sigma)(\sinh(\bar{z}_l \lambda_w) - \sinh(\bar{z}_u \lambda_w))/D \quad (23i)$$

$$237 \quad c_2 = -e^{\lambda_w}(\lambda_w + \sigma)(\sinh(\bar{z}_l \lambda_w) - \sinh(\bar{z}_u \lambda_w))/D \quad (23j)$$

$$238 \quad c_3 = \frac{e^{-(1+\bar{z}_l+\bar{z}_u)\lambda_w}}{2D} \left(\sigma(e^{(2+\bar{z}_l)\lambda_w} + e^{\bar{z}_u \lambda_w} - e^{(2\bar{z}_l+\bar{z}_u)\lambda_w}) + (\sigma - \lambda_w)e^{(\bar{z}_l+2\bar{z}_u)\lambda_w} + \lambda_w(e^{(2+\bar{z}_l)\lambda_w} - e^{\bar{z}_u \lambda_w} + e^{(2\bar{z}_l+\bar{z}_u)\lambda_w}) \right) \quad (23k)$$

$$240 \quad c_4 = \frac{e^{-(1+\bar{z}_l+\bar{z}_u)\lambda_w}}{2D} \left((\sigma - \lambda_w)e^{(\bar{z}_l+2\bar{z}_u)\lambda_w} + (\sigma + \lambda_w)(e^{(2+\bar{z}_l)\lambda_w} - e^{(2+\bar{z}_u)\lambda_w} + \right)$$

241 $e^{(2+2\bar{z}_l+\bar{z}_u)\lambda_w}) \quad (23l)$

242 $c_5 = \frac{1}{2D} e^{-(1+\bar{z}_l+\bar{z}_u)\lambda_w} (e^{\bar{z}_l\lambda_w} - e^{\bar{z}_u\lambda_w}) ((\lambda_w - \sigma) e^{(\bar{z}_l+\bar{z}_u)\lambda_w} + (\lambda_w + \sigma) e^{2\lambda_w}) \quad (23m)$

243 where $\lambda_w^2 = (\xi^2 + i\gamma)/\mu$, $\sigma = i\gamma a$, $\tilde{H}_p = 2/(\pi\mu\xi\lambda_w^2)$ and $D = 2(\sigma \cosh \lambda_w +$
 244 $\lambda_w \sinh \lambda_w)$, and $\text{Re}(-)$ is the real part of a complex number. Again, one can refer to the
 245 supporting material for the derivation of the solution. Eq. (23a) indicates SHM for the response
 246 of the hydraulic head at any point to oscillatory pumping. Note that Eq. (23f) reduces to
 247 $\bar{H}(\bar{r}, \bar{z}) = \int_0^\infty \tilde{H}_m \xi \Omega d\xi$ for a fully screened well when $\bar{z}_l = 0$ and $\bar{z}_u = 1$.

248 **2.6. Pseudo-steady state solution for confined aquifers**

249 Applying the finite Fourier cosine transform to the model, Eqs. (18) – (22) with $S_y = 0$ (i.e.,
 250 $a = 0$) for the confined condition, leads to an ordinary differential equation with two boundary
 251 conditions. With solving the boundary-value problem, the solution of \bar{h}_s for confined aquifers
 252 can be expressed as Eqs. (23a) - (23e) with $\bar{H}(\bar{r}, \bar{z})$ defined as

253 $\bar{H}(\bar{r}, \bar{z}) = -2 \sum_{m=0}^{\infty} \frac{K_0(\bar{r}\lambda_m)}{\lambda_m K_1(\lambda_m)} \times \begin{cases} 0.5(\bar{z}_u - \bar{z}_l) & \text{for } m = 0 \\ \frac{\cos(m\pi\bar{z})}{m\pi} (\sin(\bar{z}_u m\pi) - \sin(\bar{z}_l m\pi)) & \text{for } m > 0 \end{cases} \quad (24)$

254 where $\lambda_m^2 = \gamma i + \mu(m\pi)^2$. The derivation of Eq. (24) is also listed in the supporting material.
 255 For a fully screened well (i.e., $\bar{z}_u = 1$, $\bar{z}_l = 0$), the first term of the series (i.e., $m = 0$) remains
 256 and the others equal zero because of $\sin(\bar{z}_u m\pi) - \sin(\bar{z}_l m\pi) = 0$. The result is independent
 257 of dimensionless elevation \bar{z} , indicating the confined flow is only horizontal.

258 **2.7. Special cases of the present solution**

259 Table 1 classifies the present solution (i.e., Solution 1) and its special cases (i.e., Solutions 2 to
 260 6) according to transient or PSS flow, unconfined or confined aquifer, and IGD or DGD. Each
 261 of Solutions 1 to 6 reduces to a special case for fully screened well. Existing analytical solutions
 262 can be regarded as special cases of the present solution as discussed in Section 3.4 (e.g., Black
 263 and Kipp, 1981; Rasmussen et al., 2003; Dagan and Rabinovich, 2014).

264 **2.8. Sensitivity analysis**

265 Sensitivity analysis evaluates hydraulic head variation in response to the change in each of K_r ,
 266 K_z , S_s , S_y , ω , and ε . The normalized sensitivity coefficient can be defined as (Liou and Yeh,
 267 1997)

268
$$S_i = P_i \frac{\partial X}{\partial P_i} \quad (25)$$

269 where S_i is the sensitivity coefficient of i th parameter; P_i is the magnitude of the i th input
 270 parameter; X represents the present solution in dimensional form. Eq. (25) can be approximated
 271 as

272
$$S_i = P_i \frac{X(P_i + \Delta P_i) - X(P_i)}{\Delta P_i} \quad (26)$$

273 where ΔP_i , a small increment, is chosen as $10^{-3}P_i$.

274 3. Results and Discussion

275 The following sections demonstrate the response of the hydraulic head to oscillatory pumping
 276 using the present solution. The default values in calculation are $r = 0.05$ m, $z = 5$ m, $b = 10$ m,
 277 $Q = 10^{-3}$ m³/s, $r_w = 0.05$ m, $z_u = 5.5$ m, $z_l = 4.5$ m, $K_r = 10^{-4}$ m/s, $K_z = 10^{-5}$ m/s, $S_s = 10^{-5}$ m⁻¹, S_y
 278 = 10^{-4} , $\omega = 2\pi/30$ s⁻¹, and $\kappa = 100$ s. The corresponding dimensionless parameters and
 279 variables are $\bar{r} = 1$, $\bar{z} = 0.5$, $\bar{z}_u = 0.55$, $\bar{z}_l = 0.45$, $\gamma = 5.24 \times 10^{-5}$, $\mu = 2.5 \times 10^{-6}$, $a =$
 280 4×10^5 , $a_1 = 1$ and $a_2 = 2.5 \times 10^{-6}$.

281 3.1. Delayed gravity drainage

282 Previous analytical models for OPT consider either confined flow (e.g., Rasmussen et al.,
 283 2003) or unconfined flow with IGD effect (e.g., Dagan and Rabinovich, 2014). Little attention
 284 has been paid to the consideration of the DGD effect. This section addresses the difference
 285 among these three models. Figure 2 shows the curve of the dimensionless amplitude \bar{A}_t at $(\bar{r},$
 286 $\bar{z}) = (1, 1)$ of Solution 1 versus the dimensionless parameter a_1 related to the DGD effect. The
 287 transient head fluctuations are plotted based on Solution 1 with $a_1 = 10^{-2}$, 1, 10, 500,
 288 Solution 2 for IGD and Solution 3 for confined flow. Define the relative error as

289
$$RE = |\bar{A}'_t - \bar{A}_t| / \bar{A}_t \quad (27)$$

290 where \bar{A}'_t is the dimensionless amplitude predicted by Solution 2 for the case of $a_1 = 500$
 291 or Solution 3 for the case of $a_1 = 10^{-2}$. The curves of the RE versus the period of oscillatory
 292 pumping rate (i.e., P) for these two cases are displayed. The range of $P \leq 10^5$ s (1.16 d)
 293 contains most practical applications of OPT. When $10^{-2} \leq a_1 \leq 500$, the \bar{A}_t gradually
 294 decreases with a_1 to the trough and then increases to the ultimate value of $\bar{A}_t = 1.79 \times 10^{-2}$.
 295 The DGD, in other words, causes an effect. When $a_1 < 10^{-2}$, Solutions 1 and 3 agree on the
 296 predicted heads; the RE is below 1% for $P < 10^4$ s (2.78 h), indicating the unconfined aquifer
 297 with the DGD effect behaves like confined aquifer and the water table can be regarded as a no-
 298 flow boundary when $a_1 < 10^{-2}$ and $P < 10^4$ s. When $a_1 > 500$, the head fluctuations
 299 predicted by both Solutions 1 and 2 are identical; the largest RE is about 0.45%, indicating the
 300 DGD effect is ignorable and Eq. (4b) reduces to (4a) for the IGD condition. This conclusion is
 301 applicable for any magnitude of P in spite of $P > 10^5$ s.

302 3.2. Effect of finite radius of pumping well

303 Existing analytical models for OPT mostly treated the pumping well as a line source with
 304 infinitesimal radius (e.g., Rasmussen et al., 2003; Dagan and Rabinovich, 2014). The finite
 305 difference scheme for the model also treats the well as a nodal point by neglecting the radius.
 306 These will lead to significant error when a well has the radius ranging from 0.5 m to 2 m (Yeh
 307 and Chang, 2013). This section discusses the relative error in predicted amplitude defined as

$$308 RE = |\bar{A}_{D\&R} - \bar{A}_t| / \bar{A}_t \quad (28)$$

309 where \bar{A}_t and $\bar{A}_{D\&R}$ are the dimensionless amplitudes at $\bar{r} = 1$ (i.e., $r = r_w$) predicted by IGD
 310 Solution 2 and the Dagan and Rabinovich (2014) solution, respectively. Note that their solution
 311 assumes infinitesimal radius of a pumping well and has a typo that the term $e^{-D_w+1} - e^{-D_w}$
 312 should read $e^{\beta(-D_w+1)} - e^{-\beta D_w}$ (see their Eq. (25)). Figure 3 demonstrates the RE for
 313 different values of radius r_w . The RE increases with r_w as expected. For case 1 of $r_w = 0.1$ m,
 314 both solutions agree well in the entire domain of $1 \leq \bar{r} \leq \infty$, indicating a pumping well with
 315 $r_w \leq 0.1$ m can be regarded as a line source. For the extreme case 2 of $r_w = 1$ m or case 3 of

316 $r_w = 2$ m, the Dagan and Rabinovich solution underestimates the dimensionless amplitude for
317 $1 \leq \bar{r} \leq 6$ and agrees to the present solution for $\bar{r} > 6$. The *REs* for these two cases exceed
318 10%. The effect of finite radius should therefore be considered in OPT models especially when
319 observed hydraulic head data are taken close to the wellbore of a large-diameter well.

320 **3.3. Sensitivity analysis**

321 The temporal distributions of normalized sensitivity coefficient S_i defined as Eq. (26) with
322 $X = h_{\text{exp}}$ of Solution 1 are displayed in Fig. 4a for the response of exponential decay to the
323 change in each of six parameters K_r , K_z , S_s , S_y , ω and ε . The exponential decay is very sensitive
324 to variation in each of K_r , K_z , S_s and ω because of $|S_i| > 0$. Precisely, a positive perturbation
325 in S_s produces an increase in the magnitude of h_{exp} while that in K_r or K_z causes a decrease.
326 In addition, a positive perturbation in ω yields an increase in h_{exp} before $t = 1$ s and a decrease
327 after that time. It is worth noting that S_i for S_y or ε is very close to zero over the entire period
328 of time, indicating h_{exp} is insensitive to the change in S_y or ε and the subtle change of gravity
329 drainage has no influence on the exponential decay. On the other hand, the spatial distributions
330 of S_i associated with the amplitude A_t are shown in Fig. 4b in response to the changes in
331 those six parameters. The A_t is again sensitive to the change in each of K_r , K_z , S_s and ω but
332 insensitive with the change in S_y or ε . The same result of $|S_i| \cong 0$ for S_y or ε applies to any
333 observation point under the water table (i.e., $\bar{z} < 1$), but $|S_i| > 0$ at the water table (i.e., $\bar{z} =$
334 1) shown in Fig. 4c. From those discussed above, we may conclude the changes in the four key
335 parameters K_r , K_z , S_s and ω significantly affect head prediction in the entire aquifer domain.
336 The change in S_y or ε leads to insignificant variation in the predicted head below the water
337 table and slight variation at the water table.

338 **3.4. Transient head fluctuation affected by the initial condition**

339 Figure 5 demonstrates head fluctuations predicted by DGD Solution 1 and IGD Solution 2
340 expressed as $\bar{h} = \bar{h}_{\text{exp}} + \bar{h}_{\text{SHM}}$ for transient flow and by IGD solution as $\bar{h}_s = \bar{A}_s \cos(\gamma t -$
341 $\phi_s)$ for PSS flow. The transient head fluctuation starts from $\bar{h} = 0$ at $\bar{t} = 0$ and approaches

342 SHM predicted by \bar{h}_{SHM} when $\bar{h}_{\text{exp}} \cong 0$ m after $\bar{t} = 0.5\bar{P}$ (i.e., 6×10^4). Solutions 1 and
343 2 agree to the \bar{h} predictions because the head at $\bar{z} = 0.5$ under the water table is insensitive
344 to the change in S_y or ε as discussed in Section 3.3. It is worth noting that the solution of
345 Dagan and Rabinovich (2014) for PSS flow has a time shift from the \bar{h}_{SHM} of Solution 2. This
346 indicates the phase of their solution (i.e., 1.50 rad) should be replaced by the phase of Solution
347 2 (i.e., $\phi_t = 1.64$ rad) so that their solution exactly fits the \bar{h}_{SHM} of Solution 2.

348 Figure 6 displays head fluctuations predicted by transient Solution 3 expressed as $\bar{h} =$
349 $\bar{h}_{\text{exp}} + \bar{h}_{\text{SHM}}$ and PSS Solution 6 as $\bar{h}_s = \bar{A}_s \cos(\gamma t - \phi_s)$ for partially screened pumping
350 well in panel (a) and full screen in panel (b). The Rasmussen et al. (2003) solution for transient
351 flow predicts the same \bar{h} as Solution 3. The Black and Kipp (1981) for PPS flow also predicts
352 close \bar{h}_{SHM} prediction of Solution 3. The phase of Solution 6 (i.e., $\phi_s = 1.50$ rad for panel (a)
353 and 1.33 rad for (b)) can be replaced by the phase of Solution 3 (i.e., $\phi_t = 1.64$ rad for (a)
354 and 1.81 rad for (b)) so that the \bar{h}_{SHM} prediction of Solutions 3 is identical to the \bar{h}_s
355 prediction of Solution 6. As concluded, excluding the initial condition with Eq. (17) for a PSS
356 model leads to a time shift from the SHM of the head fluctuation predicted by the associated
357 transient model while the transient and PSS models give the same SHM amplitude.

358 **3.5. Application of the present solution to field experiment**

359 Rasmussen et al. (2003) conducted field OPTs in a three-layered aquifer system containing one
360 Surficial Aquifer, the Barnwell-McBean Aquifer in between and the deepest Gordon Aquifer
361 at the Savannah River site. Two clay layers dividing these three aquifers may be regarded as
362 impervious strata. For the OPT at the Surficial Aquifer, the formation has 6.25 m averaged
363 thickness near the test site. The fully-screened pumping well has 7.6 cm outer radius. The
364 pumping rate can be approximated as $Q \sin(\omega t)$ with $Q = 4.16 \times 10^{-4} \text{ m}^3/\text{s}$ and $\omega = 2\pi \text{ h}^{-1}$. The
365 distance from the pumping well is 6 m to the observation well 101D and 11.5 m to well 102D.
366 The screen lengths are 3 m from the aquifer bottom for well 101D and from the water table for
367 well 102D. For the OPT at the Barnwell-McBean Aquifer, the formation mainly consists of

368 sand and fine-grained material. The pumping well has outer radius of 7.6 cm and pumping rate
 369 of $Q\sin(\omega t)$ with $Q = 1.19 \times 10^{-3}$ m³/s and $\omega = \pi$ h⁻¹. The observation well 201C is at 6 m
 370 from the pumping well. The data of time-varying hydraulic heads at the observation wells (i.e.,
 371 101D, 102D, 201C) are plotted in Fig. 7. One can refer to Rasmussen et al. (2003) for detailed
 372 description of the Savannah River site.

373 The aquifer hydraulic parameters are determined based on Solutions 3 to 6 coupled with
 374 the Levenberg–Marquardt algorithm provided in the Mathematica function FindFit (Wolfram,
 375 1991). Note that a robust Gauss-Newton algorithm provides an alternative for the parameter
 376 estimation (Qin et al., 2018a; 2018b). Solutions 4 and 5 are used to predict depth-averaged
 377 head expressed as $(z'_u - z'_l)^{-1} \int_{z'_l}^{z'_u} h_s dz$ with the upper elevation z'_u and lower one z'_l of
 378 the finite screen of the observation well 101D or 102D at the Surficial Aquifer. Note that
 379 Solutions 3 and 6 are independent of elevation because of the fully-screened pumping well.

380 Define the standard error of estimate (SEE) as $SEE = \sqrt{\frac{1}{M} \sum_{j=1}^M e_j^2}$ and the mean error (ME)
 381 as $ME = \frac{1}{M} \sum_{j=1}^M e_j$ where e_j is the difference between predicted and observed hydraulic heads
 382 and M is the number of observation data (Yeh, 1987). The estimated parameters and associated
 383 SEE and ME are displayed in Table 2. The estimates of T , S and D_r given in Rasmussen et al.
 384 (2003) are also presented. The result shows the estimated S_y is very small, and the estimated T
 385 and S by Solution 3, 6 or the Rasmussen et al. (2003) solution for confined flow are close to
 386 those by Solution 4 or 5 for unconfined flow, indicating that the unconfined flow induced by
 387 the OPT in the Surficial Aquifer is negligibly small. Little gravity drainage due to the DGD
 388 effect appears with $a_1 = 20$ for wells 101D and 102D as discussed in Section 3.1. Rasmussen
 389 et al. (2003) also revealed the confined behaviour of the OPT-induced flow in the Surficial
 390 Aquifer. The estimated S_y is one order less than the lower limit of the typical range of 0.01 ~
 391 0.3 (Freeze and Cherry, 1979), which accords with the findings of Rasmussen et al. (2003) and
 392 Rabinovich et al. (2015). Such a fact might be attributed to the problem of the moisture

393 exchange limited by capillary fringe between the zones below and above the water table.
394 Several laboratory research outcomes have confirmed an estimate of S_y at short period of OPT
395 is much smaller than that determined by constant-rate pumping test (e.g., Cartwright et al.,
396 2003; 2005). In addition, the difference in T , S or D_r estimated by Solution 6 and those by the
397 Rasmussen et al. (2003) solution may be attributed to the fact that their solution assumes
398 isotropic hydraulic conductivity (i.e., $K_r = K_z$). On the other hand, transient Solution 3 gives
399 smaller SEEs than PSS Solution 6 or the Rasmussen et al. (2003) solution for the Barnwell-
400 McBean Aquifer and better fits to the observed data at the early pumping periods as shown in
401 Fig. 7. From those discussed above, we may conclude the present solution is applicable to real-
402 world OPT.

403 **4. Concluding remarks**

404 A variety of analytical models for OPT have been proposed so far, but little attention is paid to
405 the joint effects of DGD, initial condition, and finite radius of a pumping well. This study
406 develops a new model for describing hydraulic head fluctuation due to OPT in unconfined
407 aquifers. Static hydraulic head prior to OPT is regarded as an initial condition. A Neumann
408 boundary condition is specified at the rim of a finite-radius pumping well. A free surface
409 equation accounting for the DGD effect is considered as the top boundary condition. The
410 solution of the model is derived by the Laplace transform, finite-integral transform and Weber
411 transform. The sensitivity analysis of the head response to the change in each of hydraulic
412 parameters is performed. The observation data obtained from the OPT at the Savannah River
413 site are analyzed by the present solution when coupling the Levenberg–Marquardt algorithm
414 to estimate aquifer hydraulic parameters. Our findings are summarized below:

415 1. When $10^{-2} \leq a_1 \leq 500$, the effect of DGD on head fluctuations should be considered.
416 The amplitude of head fluctuation predicted by DGD Solution 1 decreases with increasing
417 a_1 to a trough and then increases to the amplitude predicted by IGD Solution 2. When
418 $a_1 > 500$, the DGD becomes IGD. Both Solutions 1 and 2 predict the same head

419 fluctuation. When $a_1 < 10^{-2}$ and $P < 10^4$ s, the DGD results in the water table under
420 no-flow condition. Solution 1 for unconfined flow gives an identical head prediction to
421 Solution 3 for confined flow.

422 2. Assuming a large-diameter well as a line source with infinitesimal radius underestimates
423 the amplitude of head fluctuation in the domain of $1 \leq \bar{r} \leq 6$ when the radius exceeds 80
424 cm, leading to relative error $RE > 10\%$ shown in Fig. 3. In contrast, the assumption is valid
425 in predicting the amplitude in the domain of $\bar{r} > 6$ in spite of adopting a large-diameter
426 well. When $r_w \leq 10$ cm (i.e., $RE < 0.45\%$), the well radius can be regarded as
427 infinitesimal. The result is applicable to existing analytical solutions assuming infinitesimal
428 radius and finite difference solutions treating the pumping well as a nodal point.

429 3. The sensitivity analysis suggests the changes in four parameters K_r , K_z , S_s and ω
430 significantly affect head prediction in the entire aquifer domain. The change in S_y or ε
431 causes insignificant variation in the head under water table but slight variation at the water
432 table.

433 4. Analytical solutions for OPT are generally expressed as the sum of the exponential and
434 harmonic functions of time (i.e., $\bar{h} = \bar{h}_{\text{exp}} + \bar{A}_t \cos(\gamma t - \phi_t)$) for transient solutions (e.g.,
435 Solution 3) and harmonic function (i.e., $\bar{h}_s = \bar{A}_s \cos(\gamma t - \phi_s)$) for PSS solutions (e.g.,
436 Solution 6). The latter assuming Eq. (17) without the initial condition produces a time shift
437 from the SHM predicted by the \bar{h}_{SHM} . The phase ϕ_s should be replaced by ϕ_t so that
438 \bar{h}_s and \bar{h}_{SHM} are exactly the same.

439

440 **References**

441 Bakhos, T., Cardiff, M., Barrash, W., and Kitanidis, P. K.: Data processing for oscillatory
442 pumping tests, *J. Hydrol.*, 511, 310–319, 2014.

443 Black, J. H., and Kipp, K. L.: Determination of hydrogeological parameters using sinusoidal

444 pressure tests - a theoretical appraisal, *Water Resour. Res.*, 17(3), 686–692, 1981.

445 Cardiff, M., Bakhos, T., Kitanidis, P. K., and Barrash, W.: Aquifer heterogeneity
446 characterization with oscillatory pumping: Sensitivity analysis and imaging potential, *Water*
447 *Resour. Res.*, 49(9), 5395–5410, 2013.

448 Cardiff, M. and Barrash, W.: 3-D transient hydraulic tomography in unconfined aquifers with
449 fast drainage response, *Water Resour. Res.*, 47: W12518, 2011.

450 Cardiff, M. and Barrash, W.: Analytical and semi - analytical tools for the design of oscillatory
451 pumping tests, *Ground Water*, 53(6), 896–907, 2014.

452 Cartwright, N., Nielsen, P., and Dunn, S.: Water table waves in an unconfined aquifer:
453 Experiments and modeling, *Water Resour. Res.*, 39(12), 1330, 2003.

454 Cartwright, N., Nielsen, P., and Perrochet, P.: Influence of capillarity on a simple harmonic
455 oscillating water table: Sand column experiments and modeling, *Water Resour. Res.*, 41(8),
456 W08416, 2005.

457 Christensen, N. K., Ferre, T. P. A., Fiandaca, G., and Christensen, S.: Voxel inversion of
458 airborne electromagnetic data for improved groundwater model construction and prediction
459 accuracy, *Hydrol. Earth Syst. Sci.*, 21, 1321–1337, 2017.

460 Dagan, G. and Rabinovich, A.: Oscillatory pumping wells in phreatic, compressible, and
461 homogeneous aquifers, *Water Resour. Res.*, 50(8), 7058–7066, 2014.

462 Fokker, P. A., Salina Borello, E., Serazio, C., and Verga, F.: Estimating reservoir
463 heterogeneities from pulse testing, *J. Petrol. Sci. Eng.*, 86–87, 15–26, 2012.

464 Fokker, P. A., Renner, J., and Verga, F.: Numerical modeling of periodic pumping tests in
465 wells penetrating a heterogeneous aquifer, *Am. J. Environ. Sci.*, 9(1), 1–13, 2013.

466 Freeze, R. A. and Cherry, J. A.: *Groundwater*, Prentice-Hall, New Jersey, 1979, 604 pp.

467 Kuo, C.: Determination of reservoir properties from sinusoidal and multirate flow tests in one
468 or more wells, *SPE J.*, 12(6), 499–507, 1972.

469 Latinopoulos, P.: Analytical solutions for periodic well recharge in rectangular aquifers with

470 3rd-kind boundary-conditions, *J. Hydrol.*, 77(1–4), 293–306, 1985.

471 Liang, X., Zhan, H., Zhang, Y.-K., and Liu, J.: On the coupled unsaturated-saturated flow
472 process induced by vertical, horizontal, and slant wells in unconfined aquifers, *Hydrol. Earth
473 Syst. Sci.*, 21, 1251–1262, 2017.

474 Liang, X., Zhan, H., Zhang, Y.-K., Liu, J.: Underdamped slug tests with unsaturated - saturated
475 flows by considering effects of wellbore skins, *Hydrol. Process.*, 32, 968 – 980, 2018.

476 Lin, Y.-C., Yeh, H.-D.: A lagging model for describing drawdown induced by a constant-rate
477 pumping in a leaky confined aquifer, *Water Resour. Res.*, 53, 8500 – 8511, 2017.

478 Liou, T. S., and Yeh, H. D.: Conditional expectation for evaluation of risk groundwater flow
479 and solute transport: one-dimensional analysis, *J. Hydrol.*, 199, 378–402, 1997.

480 Maineult, A., Strobach, E., and Renner, J.: Self-potential signals induced by periodic pumping
481 tests, *J. Geophys. Res: Sol. Earth*, 113(B1), B01203, 2008.

482 Moench, A. F.: Combining the Neuman and Boulton models for flow to a well in an unconfined
483 aquifer, *Ground Water*, 33(3), 378–384, 1995.

484 Muthuwatta, L., Amarasinghe, U. A., Sood, A., and Surinaidu, L.: Reviving the “Ganges Water
485 Machine”: where and how much?, *Hydrol. Earth Syst. Sci.*, 21, 2545–2557, 2017.

486 Neuman, S.P.: Theory of flow in unconfined aquifers considering delayed response of the water
487 table, *Water Resour. Res.*, 8(4), 1031–1045, 1972.

488 Povstenko, Y.: *Linear fractional diffusion-wave equation for scientists and engineers*. New
489 York, Birkhäuser, 2015.

490 Qin, Y., Kavetski, D., Kuczera, G.: A robust Gauss-Newton algorithm for the optimization of
491 hydrological models: Benchmarking against industry-standard algorithms, *Water Resour.
492 Res.*, 54(11), 9637–9654, 2018a.

493 Qin, Y., Kavetski, D., Kuczera, G.: A robust Gauss-Newton algorithm for the optimization of
494 hydrological models: From standard Gauss-Newton to robust Gauss-Newton, *Water Resour.
495 Res.*, 54(11), 9655–9683, 2018b.

496 Rabinovich, A., Barrash, W., Cardiff, M., Hochstetler, D., Bakhos, T., Dagan, G., and Kitanidis,
497 P. K.: Frequency dependent hydraulic properties estimated from oscillatory pumping tests
498 in an unconfined aquifer, *J. Hydrol.*, 531, 2–16, 2015.

499 Rasmussen, T. C., Haborak, K. G., and Young, M. H.: Estimating aquifer hydraulic properties
500 using sinusoidal pumping at the Savannah River site, South Carolina, USA, *Hydrogeol. J.*,
501 11(4), 466–482, 2003.

502 Spane, F. A. and Mackley, R. D.: Removal of river-stage fluctuations from well response using
503 multiple regression, *Ground Water*, 49(6), 794–807, 2011.

504 Vine, N. L., Butler, A., McIntyre, N., and Jackson, C.: Diagnosing hydrological limitations of
505 a land surface model: application of JULES to a deep-groundwater chalk basin, *Hydrol.*
506 *Earth Syst. Sci.*, 20, 143–159, 2016.

507 Watlet, A., Kaufmann, O., Triantafyllou, A., Poulain, A., Chambers, J. E., Meldrum, P. I.,
508 Wilkinson, P. B., Hallet, V., Quinif, Y., Ruymbeke, M. V., and Camp, M. V.: Imageing
509 groundwater infiltration dynamics in the karst vadose zone with long-term ERT monitoring,
510 *Hydrol. Earth Syst. Sci.*, 22, 1563–1592, 2018.

511 Wolfram, S.: *Mathematica*, Version 2.0. Wolfram Research, Inc., Champaign, IL, 1991.

512 Yeh, H. D.: Theis' solution by nonlinear least - squares and finite - difference Newton's
513 Method, *Ground Water*, 25(6), 710–715, 1987.

514 Yeh, H. D., Chang, Y. C.: Recent advances in modeling of well hydraulics, *Adv. Water Resour.*
515 51, 27 – 51, 2013.

516 Yeh, T. C. J. and Liu, S. Y.: Hydraulic tomography: Development of a new aquifer test method,
517 *Water Resour. Res.*, 36(8), 2095–2105, 2000.

518 Zhou, Y. Q., Lim, D., Cupola, F., and Cardiff, M.: Aquifer imaging with pressure waves
519 evaluation of low-impact characterization through sandbox experiments, *Water Resour. Res.*,
520 52(3), 2141–2156, 2016.

521 **Acknowledgments**

522 Research leading to this paper has been partially supported by the grants from the Fundamental
523 Research Funds for the Central Universities (2018B00114), the National Natural Science
524 Foundation of China (51809080, 51879068, and 41561134016), National Key Research and
525 Development Program (2018YFC0407900), and the Taiwan Ministry of Science and
526 Technology under the contract numbers MOST 107-2221-E-009-019-MY3. The authors are
527 grateful to Prof. T. C. Rasmussen for kindly providing the OPT data obtained from the
528 Savannah River site.

Table 1. The present solution and its special cases

Well screen	Transient flow		Pseudo-steady state flow	
	Unconfined aquifer	Confined aquifer	Unconfined aquifer	Confined aquifer
Partial	Solutions 1 and 2	Solution 3	Solutions 4 and 5	Solution 6
Full	Solutions 1 and 2 ^a	Solution 3 ^{a,b}	Solutions 4 and 5 ^a	Solution 6 ^{a,b}

530 Solution 1 consists of Eqs. (14a) – (14k) with the roots of Eq. (15) and $c_0 = a_1 p_0 / (p_0 + a_2)$ for DGD.

531 Solution 2 is the same as Solution 1 but has $c_0 = a p_0$ for IGD.

532 Solution 3 equals Solution 1 with Eqs. (16a) – (16d) and $\beta_n = 0, \pi, 2\pi, \dots, n\pi$.

533 Solution 4 is the component \bar{h}_{SHM} of Solution 1 for DGD.

534 Solution 5 consists of Eqs. (23a) – (23m) for IGD.

535 Solution 6 consists of Eqs. (23a) – (23e) with $\bar{H}(\bar{r}, \bar{z})$ defined by Eq. (24).

536 ^a $\bar{z}_u = 1$ and $\bar{z}_l = 0$ for fully screened well

537 ^b The solution is independent of elevation.

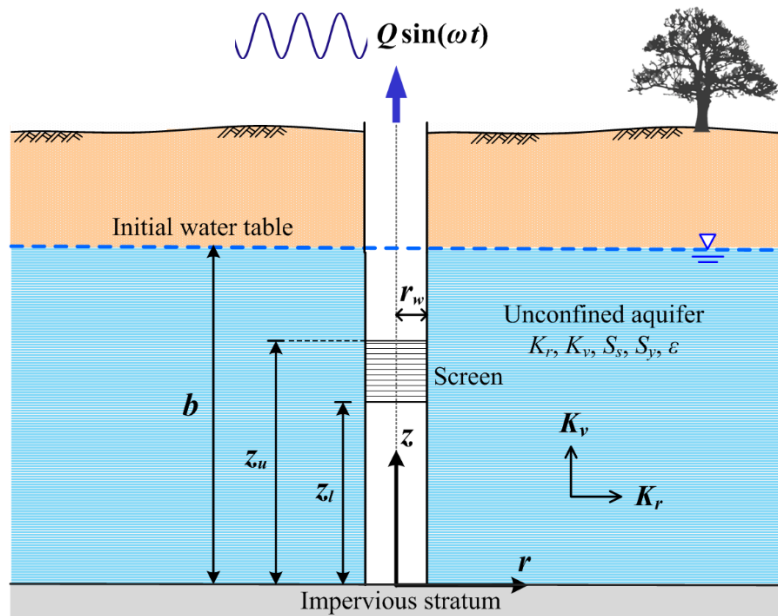
538

Table 2. Hydraulic parameters estimated by the present solution and the Rasmussen et al. (2003) solution for OPT data from the Savannah River site

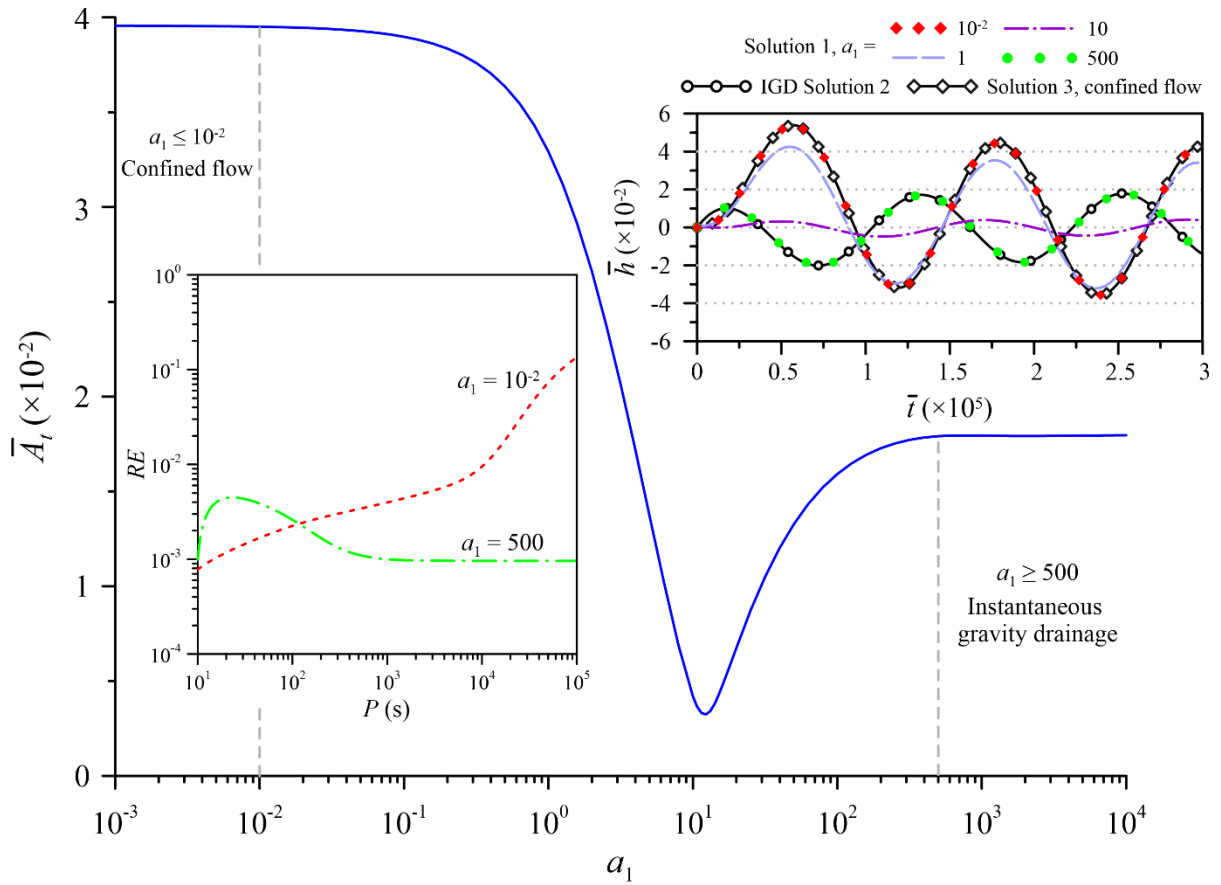
Observation well	Solution	T (m ² /s)	S	D_r (m ² /s)	K_z (m/s)	S_y	C_y (m/s)	α	κ (s)	SEE	ME
<i>Surficial Aquifer</i>											
101D	Solution 3 ^a	9.27×10^{-4}	2.44×10^{-3}	0.380	-	-	-	-	-	0.018	-5.56×10^{-3}
	Solution 6 ^b	9.18×10^{-4}	2.33×10^{-3}	0.393	-	-	-	-	-	0.018	-2.20×10^{-4}
	Solution 4 ^c	4.61×10^{-4}	3.95×10^{-3}	0.117	7.38×10^{-6}	2.23×10^{-3}	3.31×10^{-3}	0.10	94.34	0.018	-2.20×10^{-4}
	Solution 5 ^c	5.25×10^{-4}	1.09×10^{-3}	0.482	2.61×10^{-5}	5.49×10^{-3}	4.75×10^{-3}	0.31	-	0.019	-2.30×10^{-4}
	Rasmussen et al. (2003) ^b	2.17×10^{-3}	1.35×10^{-4}	16.074	-	-	-	-	-	0.018	-2.20×10^{-4}
102D	Solution 3 ^a	9.13×10^{-4}	1.76×10^{-3}	0.519	-	-	-	-	-	0.010	-4.38×10^{-3}
	Solution 6 ^b	9.17×10^{-4}	1.67×10^{-3}	0.549	-	-	-	-	-	0.011	9.57×10^{-4}
	Solution 4 ^c	9.57×10^{-5}	7.85×10^{-4}	0.122	3.68×10^{-6}	4.95×10^{-3}	7.43×10^{-4}	0.24	420.17	0.011	9.57×10^{-4}
	Solution 5 ^c	9.49×10^{-5}	3.25×10^{-4}	0.292	4.67×10^{-6}	4.68×10^{-3}	9.98×10^{-4}	0.31	-	0.011	9.50×10^{-4}
	Rasmussen et al. (2003) ^b	2.27×10^{-3}	2.28×10^{-4}	9.956	-	-	-	-	-	0.011	9.57×10^{-4}
<i>Barnwell-McBean Aquifer</i>											
201C	Solution 3 ^a	5.86×10^{-5}	7.07×10^{-4}	0.083	-	-	-	-	-	0.232	0.046
	Solution 6 ^b	6.03×10^{-5}	6.54×10^{-4}	0.092	-	-	-	-	-	0.363	0.281
	Rasmussen et al. (2003) ^b	6.90×10^{-5}	4.74×10^{-4}	0.150	-	-	-	-	-	0.363	0.281

540 ^a transient confined flow541 ^b PSS confined flow542 ^c PSS unconfined flow

Figures



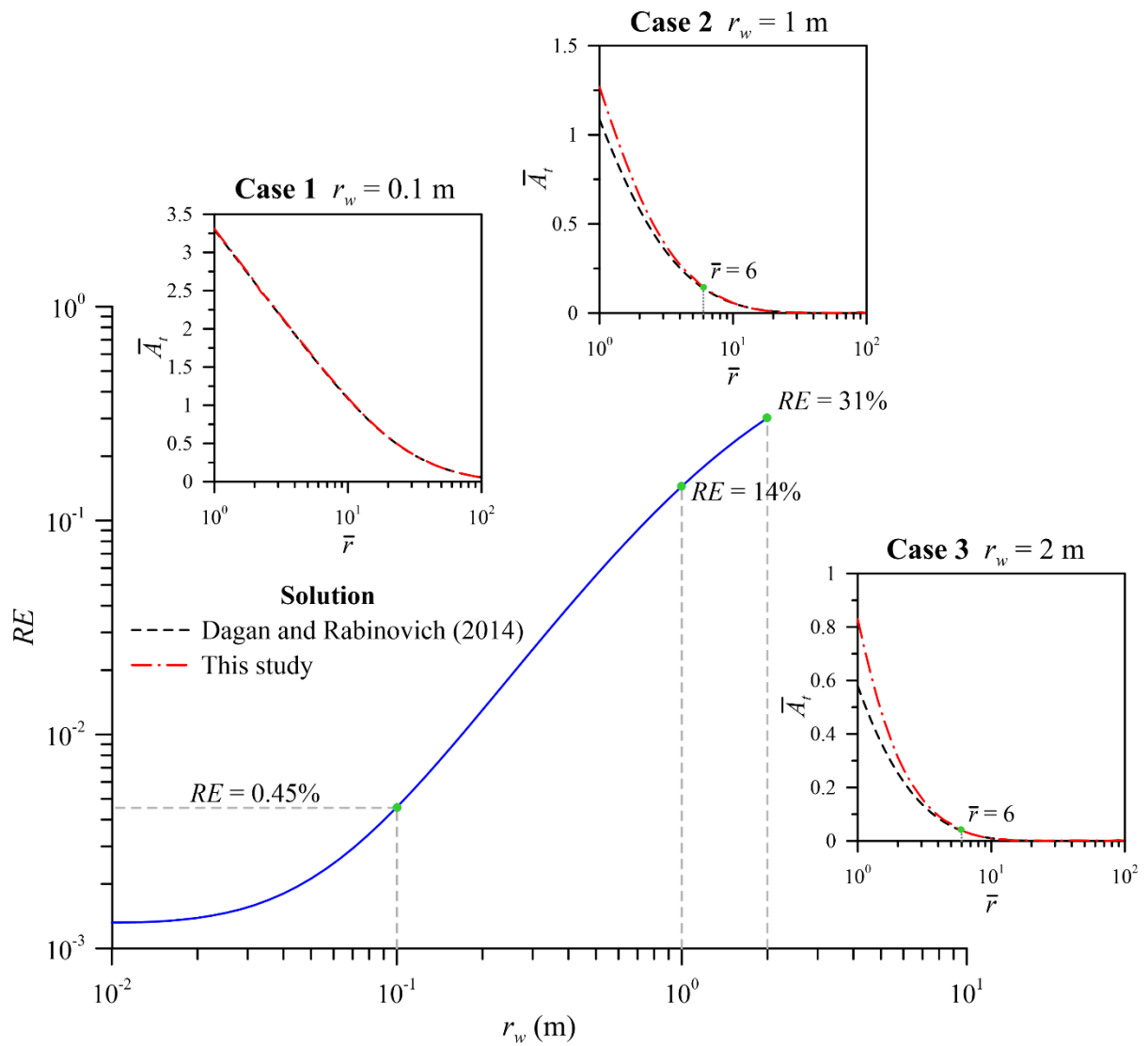
545 **Figure 1.** Schematic diagram for oscillatory pumping test at a partially screened well of finite
546 radius in an unconfined aquifer.



547

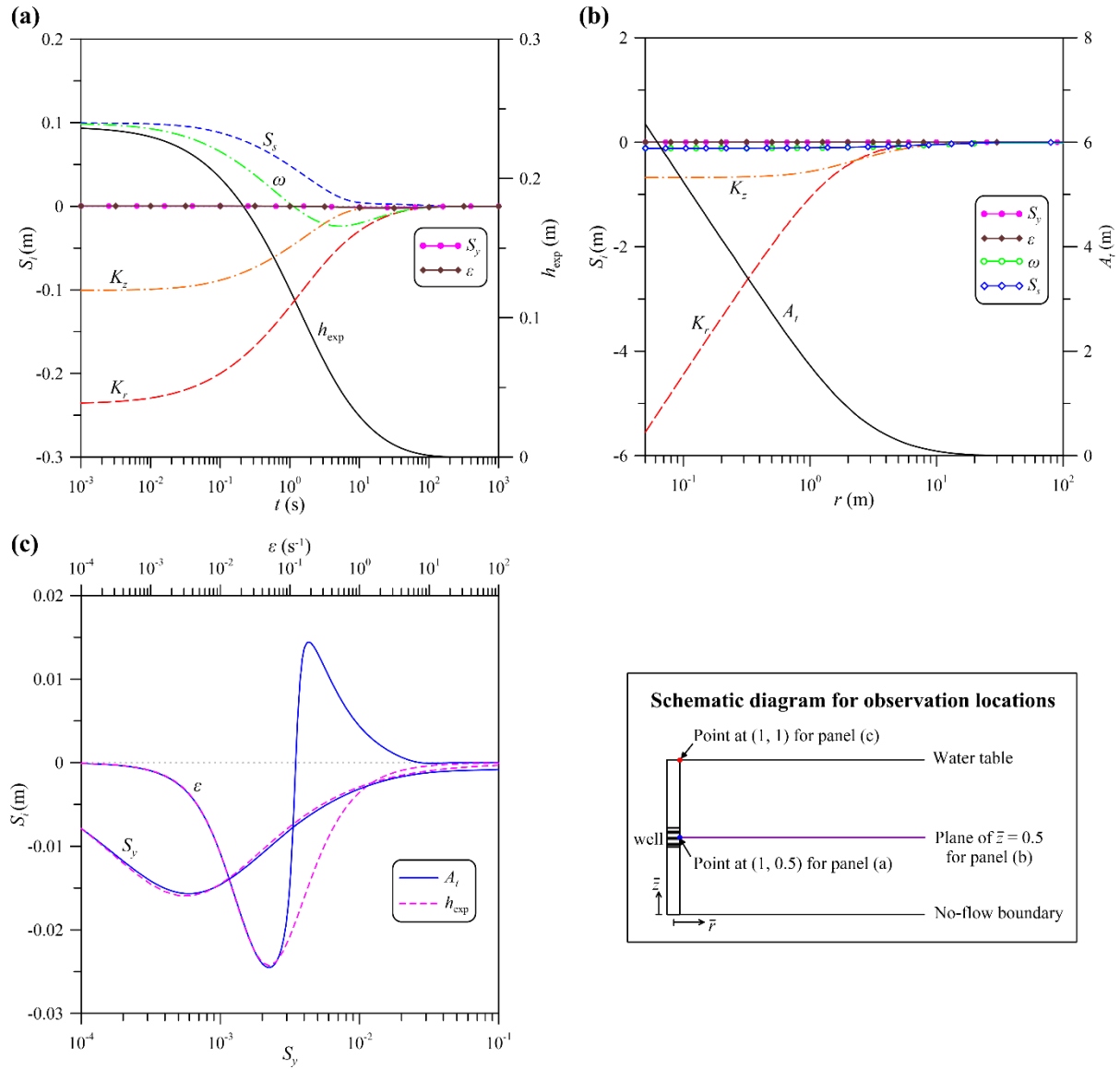
548 **Figure 2.** Influence of delayed gravity drainage on the dimensionless amplitude \bar{A}_t and
 549 transient head \bar{h} at $\bar{r} = 1$, $\bar{z} = 1$ predicted by Solution 1 for different magnitudes of a_1
 550 related to the influence.

551



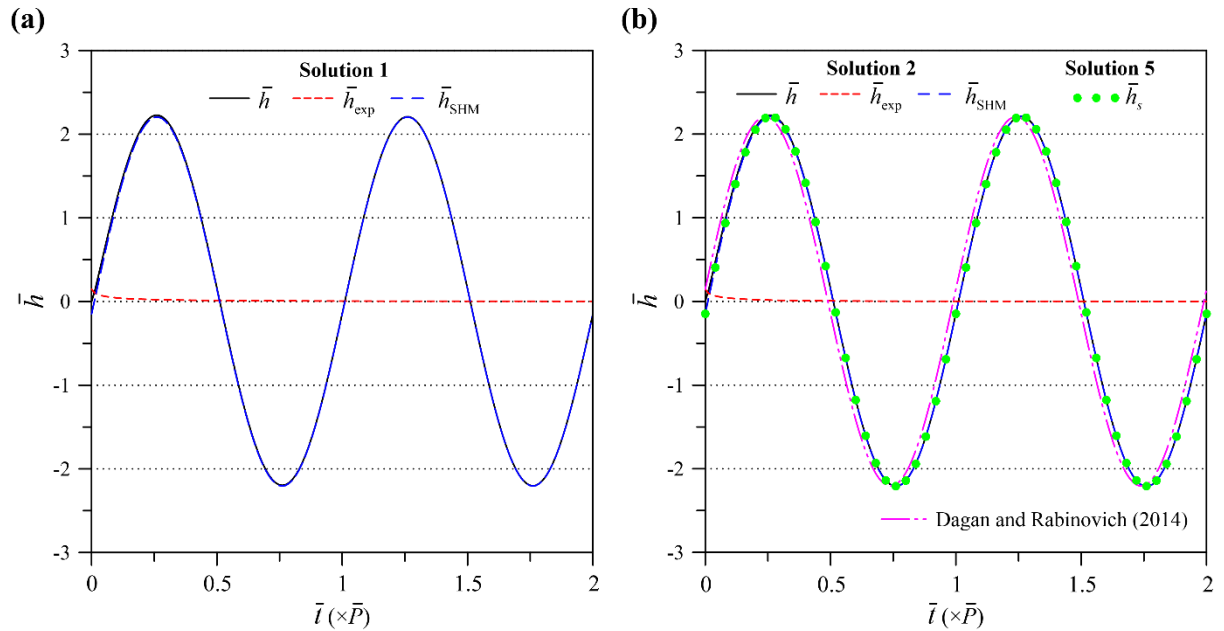
552

553 **Figure 3.** Relative error (RE) on the dimensionless amplitudes \bar{A}_t at the rim of the pumping
 554 well (i.e., $r = r_w$) predicted by IGD Solution 2 and the Dagan and Rabinovich (2014) solution.
 555 The well radius is assumed infinitesimal in the Dagan and Rabinovich (2014) solution and
 556 finite in our solution.



557

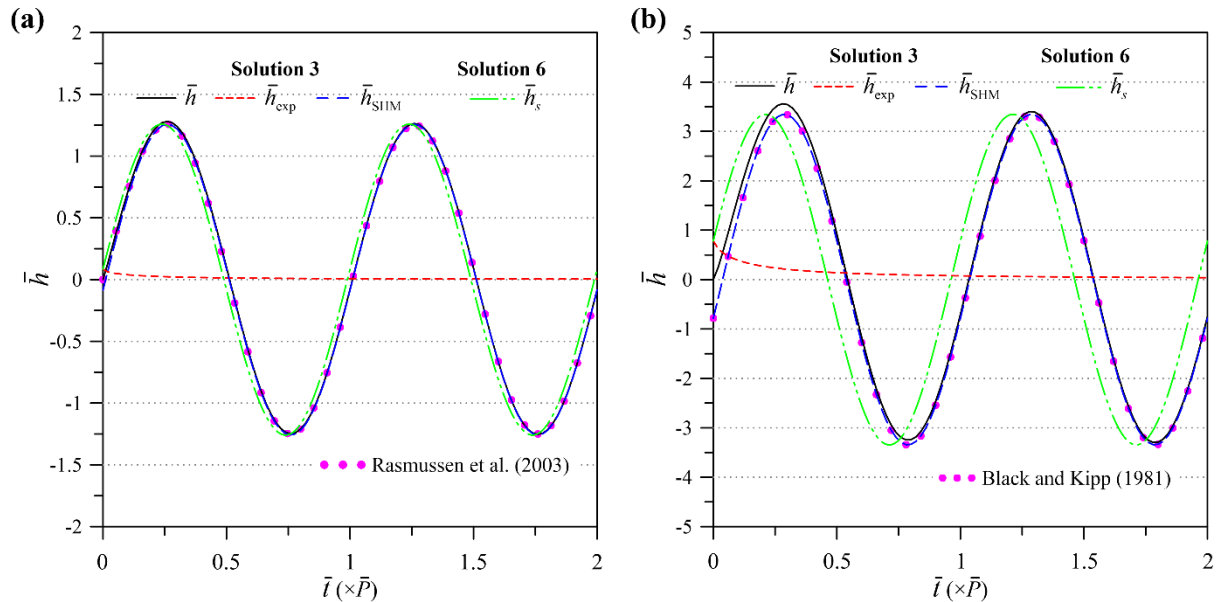
558 **Figure 4.** The normalized sensitivity coefficient S_i associated with (a) the exponential
559 component h_{exp} of Solution 1 and (b) the SHM amplitude A_t for parameters K_r , K_z , S_s , S_y , ω and
560 ϵ . The observation locations for panels (a) and (b) are under water table (i.e., $\bar{z} = 0.5$). Panel
561 (c) displays the curves of S_i of h_{exp} and A_t at water table (i.e., $\bar{z} = 1$) versus S_y and ϵ .
562



563

564 **Figure 5.** Heads fluctuations at $\bar{r} = 6$ predicted by (a) DGD Solution 1 and (b) IGD Solution
 565 2. Solutions 1 and 2 are expressed as $\bar{h} = \bar{h}_{\text{exp}} + \bar{h}_{\text{SHM}}$ for transient flow. IGD Solution 5
 566 expressed as $\bar{h}_s = \bar{A}_s \cos(\gamma t - \phi_s)$ accounts for PSS flow.

567



568

569 **Figure 6.** Heads fluctuations at $\bar{r} = 6$ predicted by Solutions 3 and 6 for (a) partially-screened
 570 pumping well and (b) fully-screened pumping well. Solution 3 is expressed as $\bar{h} = \bar{h}_{\text{exp}} +$
 571 \bar{h}_{SHM} for transient flow. Solution 6 expressed as $\bar{h}_s = \bar{A}_s \cos(\gamma t - \phi_s)$ accounts for PSS
 572 flow.

573

